Nanoscale Advances

ROYAL SOCIETY OF CHEMISTRY

PAPER

View Article Online
View Journal | View Issue

Cite this: *Nanoscale Adv.*, 2025, **7**, 4929

Protein corona composition modulates uptake of polymeric micelles by colorectal cancer cells†

Munira Sirazum,[a] Ahmed Abdelfattah,[ab] Prashant Pandey,[ac] Aliakbar Ashkarran,[defg] Soheyl Tadjiki,[h] Shahriar Sharifi,[de] Hassan Gharibi,[i] Amir Ata Saei,[j] Morteza Mahmoudi *[de] and Afsaneh Lavasanifar *[ac]

Protein corona formation on nanoparticles affects their biological interactions and fate. Polymeric micelles (PMs), preferred nanocarriers for poorly water-soluble drugs, have unclear behaviors in biological environments. This study examines the protein corona compositions of PMs formed from poly(ethylene oxide)-*block*-poly(ε-caprolactone) (PEO–PCL) and PEO-*block*-poly(α-benzyl carboxylate-ε-caprolactone) (PEO–PBCL) copolymers with varying degrees of polymerization after incubation in human plasma, and explores their relationship with cellular uptake by colorectal cancer cells. Traceable block copolymers were synthesized, self-assembled into PMs (44–99 nm, slightly negative zeta potentials), and characterized. Protein coronas were formed by incubating PMs with human plasma; protein-coated micelles were separated and analyzed. Uptake of selected PMs, with and without human plasma pre-incubation, by colorectal cancer cells was assessed. PEO–PCL micelles exhibited higher cellular uptake than PEO–PBCL micelles. Human plasma significantly reduced the uptake of PEO–PCL micelles, while PEO–PBCL micelles' uptake remained low. Proteomic analysis identified 23 distinct proteins among the combined top 20 most abundant proteins from each PM corona, with 18 common across all micelle types. In the top 10 proteins, PEO–PCL micelles shared an identical profile, whereas PEO–PBCL micelles had two unique proteins not present in PEO–PCL coronas. Protein corona composition in both PMs was shown to influence their cellular uptake behavior.

Received 30th December 2024
Accepted 5th June 2025

DOI: 10.1039/d4na01085j

rsc.li/nanoscale-advances

Introduction

Biodegradable polymeric micelles (PMs), have been extensively studied as vehicles for drug delivery.[1] Polymeric micelles are formed by the self-assembly of amphiphilic block copolymers in an aqueous environment, resulting in a core–shell structure, where the hydrophobic core acts as a nano-reservoir for the therapeutic agents, and the hydrophilic shell interfaces the media.[2,3] These systems enhance the solubility, stability, and pharmacokinetics of poorly water-soluble drugs.[4–6] The pharmacokinetics and biodistribution of their encapsulated cargo can be influenced by several factors, including the physicochemical properties of the PMs, such as size, size distribution, morphology, thermodynamic and kinetic stability, and the payload release rate. An important phenomenon in this context is the formation of the protein corona and its composition.[7]

Upon introduction of nanocarriers into the bloodstream, depending on their structure, different plasma proteins are rapidly adsorbed onto the surface of nanocarriers, forming a coating known as the protein corona.[8,9] This is a dynamic process that begins with the adsorption of the most abundant proteins, which are often replaced over time by proteins with higher binding affinities—a phenomenon referred to as the Vroman effect.[10,11] The composition and structure of the protein corona are influenced by various factors, including the size,[12–15] shape,[16] surface chemistry,[17] hydrophobicity, and charge[13,14,18] of the nanocarriers, as well as the characteristics of the biological environment.[15] The protein corona is often described as

[a]*Faculty of Pharmacy and Pharmaceutical Sciences, University of Alberta, Edmonton, Alberta T6G 2E1, Canada. E-mail: afsaneh@ualberta.ca; Fax: +1 7804921217; Tel: +1 7804922742*

[b]*Department of Industrial Pharmacy, Faculty of Pharmacy, Assiut University, Assiut, 71526, Egypt*

[c]*Department of Pharmaceutical Sciences, Babasaheb Bhimrao Ambedkar University, Lucknow, Uttar Pradesh 226025, India*

[d]*Precision Health Program, Michigan State University, East Lansing, MI, USA. E-mail: mahmou22@msu.edu; Tel: +1 5173530543*

[e]*Department of Radiology, College of Human Medicine, Michigan State University, MI, USA*

[f]*Department of Physics and Energy Science, University of Colorado, Colorado Springs, CO, USA*

[g]*BioFrontiers Center, University of Colorado, Colorado Springs, CO, USA*

[h]*Postnova Analytics Inc., Salt Lake City, UT 84102, USA*

[i]*Division of Chemistry I, Department of Medical Biochemistry and Biophysics, Karolinska Institutet, Stockholm, Sweden*

[j]*Center for Translational Microbiome Research, Department of Microbiology, Tumor and Cell Biology, Karolinska Institutet, Stockholm 17165, Sweden*

† Electronic supplementary information (ESI) available. See DOI: https://doi.org/10.1039/d4na01085j

a unique fingerprint for each nanoparticle type,[19,20] and plays a critical role in defining the biological identity of nanocarriers and how nanocarriers are perceived by different components of the biological environment.[21] This identity directly impacts critical biological processes, such as cellular uptake, circulation lifetime, clearance, and targeting capacity of nanocarriers.[22] For example, proteins in the corona shell can interact with specific cell receptors (*e.g.*, integrin),[13] guiding nanoparticles uptake by particular cells or tissues. Moreover, protein corona can also cause unintended interactions such as rapid clearance or off-target effects, potentially compromising the effectiveness of the nanocarriers.[23,24]

In the past two decades,[25] several studies have been carried out to understand the protein corona formed on nanocarriers[26–28] including polystyrene, poly(lactide-*co*-glycolide), and metallic nanoparticles.[29] Despite significant progress in characterizing the protein corona of some polymer-based nanoparticles,[30] several gaps remain in understanding the relationship between the structure of polymers making the nanoparticles and their protein corona profile as well as the ultimate effect of protein corona composition on the extent and kinetics of nanoparticle uptake by their target cells. Both PEO–PCL and PEO–PBCL micelles have attracted attention as potential nanocarriers, mainly due to their biocompatibility, biodegradability, and high payload encapsulation efficiency.[31–38] In a previous study, Garg *et al.*[39] briefly investigated how the degree of polymerization (DP) or chain length of the core-forming blocks in PEO–PCL and PEO–PBCL micelles influenced the extent of protein adsorption following exposure to fetal bovine serum (FBS). However, a detailed analysis of the protein corona or its impact on cellular uptake of PMs was beyond the scope of their study and, therefore, was not investigated in detail. Another study by Li *et al.*[30] investigated the effect of FBS on the cellular uptake of PEO–PCL nanocarriers with increasing PCL lengths, but their protein corona profiles were not analysed. In the current study, we conducted a comprehensive investigation of the effect of the core-forming block on the protein corona composition of PEO–PCL and PEO–PBCL micelles of defined DPs in their hydrophobic core-forming blocks. Moreover, the interplay between polymer structure, protein corona composition, and uptake of PEO–PCL as well as PEO–PBCL micelles by colorectal cancer (CRC) cells was assessed. CRC is a molecularly heterogeneous cancer. Profiling the protein corona of nanomedicine-based treatments for colorectal cancers (CRCs) is crucial for identifying optimized nanocarriers, enabling improved treatment outcomes in CRC patients through precision medicine.

Results

Characterization of synthesized block copolymers

We investigated a total of seven block copolymers containing hydrophilic PEO blocks (DP 114, MW 5000 Da) and either PCL or PBCL hydrophobic blocks of different chain lengths. The characteristics of prepared block copolymers in terms of DP of the hydrophobic block, and molecular weight (MW) as analysed by ^{1}H NMR (MW) and GPC (M_n), dispersity ($Đ$), and conjugation efficiency of the Cy5.5 dye to the block copolymers are reported in Table 1. In this table and throughout the manuscript, block copolymers were denoted based on their hydrophobic block segment, followed by their corresponding DPs. The DP of α-propargyl carboxylate-ε-caprolactone (PCC) in PEO–PCL–PCC and PEO–PBCL–PCC tri-block copolymers after end-capping with PCC was determined from the ^{1}H NMR and was found to be 3 in all the seven block copolymers under study. The dispersity ($Đ$) of PBCL-containing block copolymers decreased with an increase in the DP of the hydrophobic segment of the block copolymer. However, no such trend was observed for PCL-containing block copolymers.

Characterization of PMs

Four micelles that are prepared from the PEO–PCL block copolymers (PEO_{114}–PCL_{19}, PEO_{114}–PCL_{43}, PEO_{114}–PCL_{64}, and PEO_{114}–PCL_{79}) are denoted as PCL19, PCL43, PCL64, and

Table 1 Characteristics of the PEO-*b*-PCL and PEO-*b*-PBCL di-block copolymers and micelles under study

Block copolymer	PEO_{114}–PCL_{19}	PEO_{114}–PCL_{43}	PEO_{114}–PCL_{64}	PEO_{114}–PCL_{79}	PEO_{114}–$PBCL_{19}$	PEO_{114}–$PBCL_{35}$	PEO_{114}–$PBCL_{60}$
Denoted by	PCL19	PCL43	PCL64	PCL79	PBCL19	PBCL35	PBCL60
DP (degrees of polymerization) of the hydrophobic block	19	43	64	79	19	35	60
MW of the of the hydrophobic block	2166	4902	7616	9059	4712	8620	14 788
MW[a] (g mol^{-1})	7166	9902	12 616	14 059	9712	13 620	19 788
M_n[b] (g mol^{-1})	6918	8595	12 335	14 775	9115	12 288	21 770
Dispersity ($Đ = M_w/M_n$)	2.331	1.268	1.316	1.74	2.159	1.899	1.426
Fraction of PEO, f_{EO} [$f_{EO} = MW_{PEO}/MW_{entire}$]	0.70	0.50	0.4	0.36	0.51	0.37	0.25
Cy5.5 conjugation efficiency (%)	15.6 ± 2.3	20.8 ± 3.4	22.4 ± 1.4	23.9 ± 0.4	27.5 ± 2.8	21.7 ± 2.4	52.2 ± 0.9
Average diameter by DLS (nm)	99 ± 0.79	68 ± 0.49	63 ± 0.29	44 ± 0.38	45 ± 0.35	83 ± 0.18	66 ± 0.37
PDI	0.18	0.29	0.12	0.17	0.22	0.15	0.28
Average diameter by TEM (nm)	15.7 ± 7.5	26.7 ± 20.3	27.9 ± 11.2	32 ± 15.7	15.7 ± 7.5	30.9 ± 7.4	29.6 ± 8.4
Zeta potential (ZP) (mV)	−9.3 ± 0.7	−16.5 ± 0.2	−16.4 ± 1	−21.1 ± 0.4	−5.4 ± 0.1	−10.84 ± 0.6	−11.92 ± 0.7

[a] From ^{1}H NMR. [b] From GPC.

PCL79, respectively, throughout the manuscript. Similarly, micelles from the PEO–PBCL block copolymers (PEO_{114}–$PBCL_{19}$, PEO_{114}–$PBCL_{35}$, and PEO_{114}–$PBCL_{60}$) are denoted as PBCL19, PBCL35, and PBCL60, respectively. The average size of micelles containing PCL blocks decreased significantly as the DP of the PCL block increased (Fig. S1†). The zeta potential values of the PMs were slightly negative. A strong correlation was observed between the DP of the core-forming blocks of the polymers and the zeta potential of the corresponding micelles (Fig. S2†). Specifically, as the DP of the core-forming hydrophobic block increased, the zeta potential of the micelles became more negative.

The transmission electron microscopy (TEM) images of the polymeric micelles in Fig. 1 show worm-like or rod-like morphologies for PCL19 and PCL43, spherical morphologies for PCL64, PCL79, and PBCL19, while PBCL35 and PBCL60 displayed a mixture of spherical and rod-like structure. The dark spots visible in PCL19 are staining artifacts usually resulted from the variations in sample drying. Similar to our observations with the DLS measurements, the average sizes measured by TEM showed to significantly increase with increasing the DP of the hydrophobic blocks in the PEO–PCL micelles. This trend was not observed for PEO–PBCL micelles.

Fluorescent labeling of PMs through Cy5.5-conjugation

Cy5.5 conjugation efficiency was between 15.6 ± 2.3 (for PCL19), and 52.2 ± 0.9 (PBCL60). The remaining polymers exhibited similar conjugation efficiencies ranging between 20.8 ± 3.4 and 27.5 ± 2.8. The composition of PMs for each polymer is listed in Table S1.† Most of the PMs under study did not exhibit a significant release of Cy5.5 dye when incubated in DMEM media for 24 h, with the exceptions being PCL19 and PBCL19 micelles, as illustrated in Fig. S5.† These micelles demonstrated a release of 18 and 7.6% of the dye under these conditions, respectively. These two polymers were further studied for a 6 h release period, where PCL19 and PBCL19 revealed no notable dye release during the 6 h release period in media (Fig. S5†). This evidence indicates the Cy5.5 fluorophore conjugated to the block copolymers remains attached to them to make the PMs traceable within the duration of the cell uptake study. In other words, the fluorescence observed in the cellular uptake experiments can be attributed to the uptake of the PMs by the cells rather than the uptake of free Cy5.5 dye.

In vitro uptake by CRC cells in culture media with 10% FBS

HCT116 and SW620 cells were used in the study. HCT116 is derived from a primary colorectal cancer, with aggressive growth and doubling time between 20–24 hours,[40] while SW620 is derived from lymph-nodes metastasis, mimicking the behavior of metastatic and chemo-resistant cancer cells, which are critical targets for advanced drug delivery systems.[41] These two cell lines are often used as model cell lines for studying the cellular uptake of nanoparticles.

In general, PEO–PCL micelles showed higher cellular uptake in terms of median fluorescence intensities (MFI) compared to PEO–PBCL micelles in both cell lines under study (Fig. 2 and S6†). Although no specific correlation between the core-forming block lengths of PEO–PCL micelles and cell uptake could be drawn, both HCT116 and SW620 cell lines showed significantly higher uptake of PCL19 micelles. Overall, cell uptake was higher after 24 h compared to 6 h incubation for all PCL-containing PMs.

For PBCL micelles, as the DP of the hydrophobic blocks increased, their cellular uptake significantly decreased in both cell lines. Uptake by the HCT116 cell line was higher than the SW620 cell line. Additionally, PEO–PBCL micelles showed a negligible difference in cellular uptake between 6 and 24 h incubation times in FBS-containing medium in both cell lines.

In vitro cellular uptake in the presence and absence of human plasma

In this study, our objective was to analyse the protein corona formed around the polymeric micelles after incubation with human plasma and study their cellular uptake behavior to

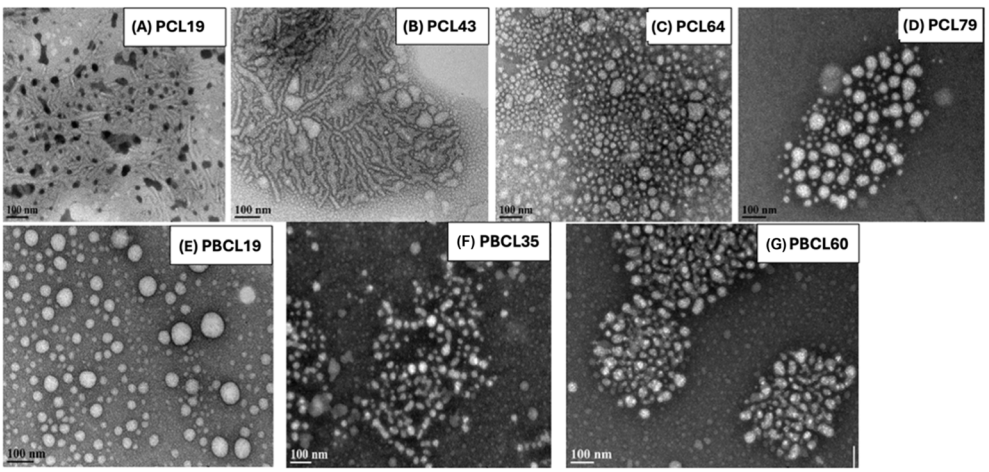

Fig. 1 Transmission electron microscopy (TEM) images of PMs made from block copolymers under study. The bar in the bottom left corner of each image indicates a scale of 100 nm.

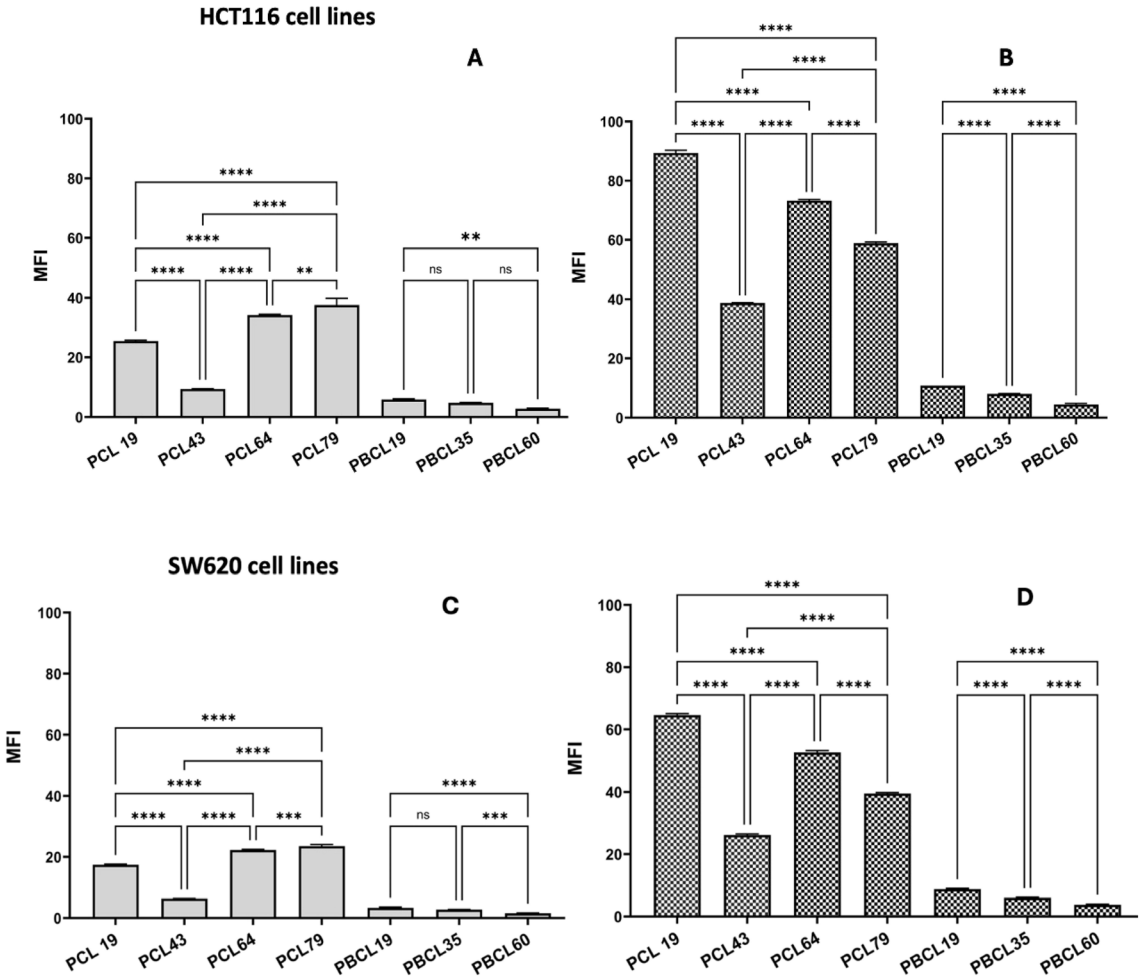

Fig. 2 Cellular uptake of Cy5.5-labelled PEO–PCL and PEO–PBCL micelles after (A) 6 h and (B) 24 h by HCT116, (C) 6 h, and (D) SW620 cells in FBS-containing media (solid bars and checkered bars show 6 h and 24 h treatments, respectively). Data from three independent experiments were compared by one-way ANOVA multiple comparison test following Tukey's method (*$p \leq 0.05$, **$p \leq 0.01$, ***$p \leq 0.001$, ****$p \leq 0.0001$).

investigate if the variation in the proteins isolated from the specific micelles impacts the cellular uptake pattern. For this, we selected three specific micelles—PCL6, PCL79, and PBCL19—to study their cellular uptake behavior in the presence and absence of human plasma. These same micelles were selected for in-depth protein corona studies. The primary selection criterion for these micelles was the ability to obtain accurate and robust characterization of their protein corona. Our results using the FFF approach demonstrated that the data for these three formulations are reliable, as other compounds exhibited micelle aggregation during protein corona formation, indicating that the selected PMs produced consistent and trustworthy protein corona profiles. The other four micelles were excluded because of forming aggregates or displaying random coil shapes during preliminary FFF analysis (Fig. S7 and S8 of the ESI†), making them unsuitable for accurate protein corona characterization. We used pooled human plasma as it avoids consideration of personalized plasma protein variation and therefore can provide more reliable results for the purpose of this study. Besides, it provides a closer approximation of the *in vivo* conditions compared to serum, enabling more accurate predictions of nanoparticle behavior inside the body in terms of protein corona formation in plasma.[42] The PEO–PCL micelles incubated with pooled human plasma during the cell uptake study showed a significant reduction in uptake compared to plasma-free culture media in both cell lines (Fig. 3).

In contrast, PBCL19 micelles did not show any significant difference in cellular uptake, irrespective of the presence or absence of human plasma in either cell line. The cell uptake for PEO–PBCL micelles remained low in both cell lines with or without incubation with human plasma. Overall, uptakes in 24 h treatments were higher than 6 h treatment for PEO–PCL micelles in both cell lines. For PBCL19 micelles, 24 h uptake was higher in HCT116 cells, but no significant difference was observed in SW620 cells compared to the 6 h.

Characteristics of the protein corona on the PMs

Isolating protein corona-coated PMs using standard centrifugation techniques proved challenging due to the similarity in density between the coated PMs and the protein source from

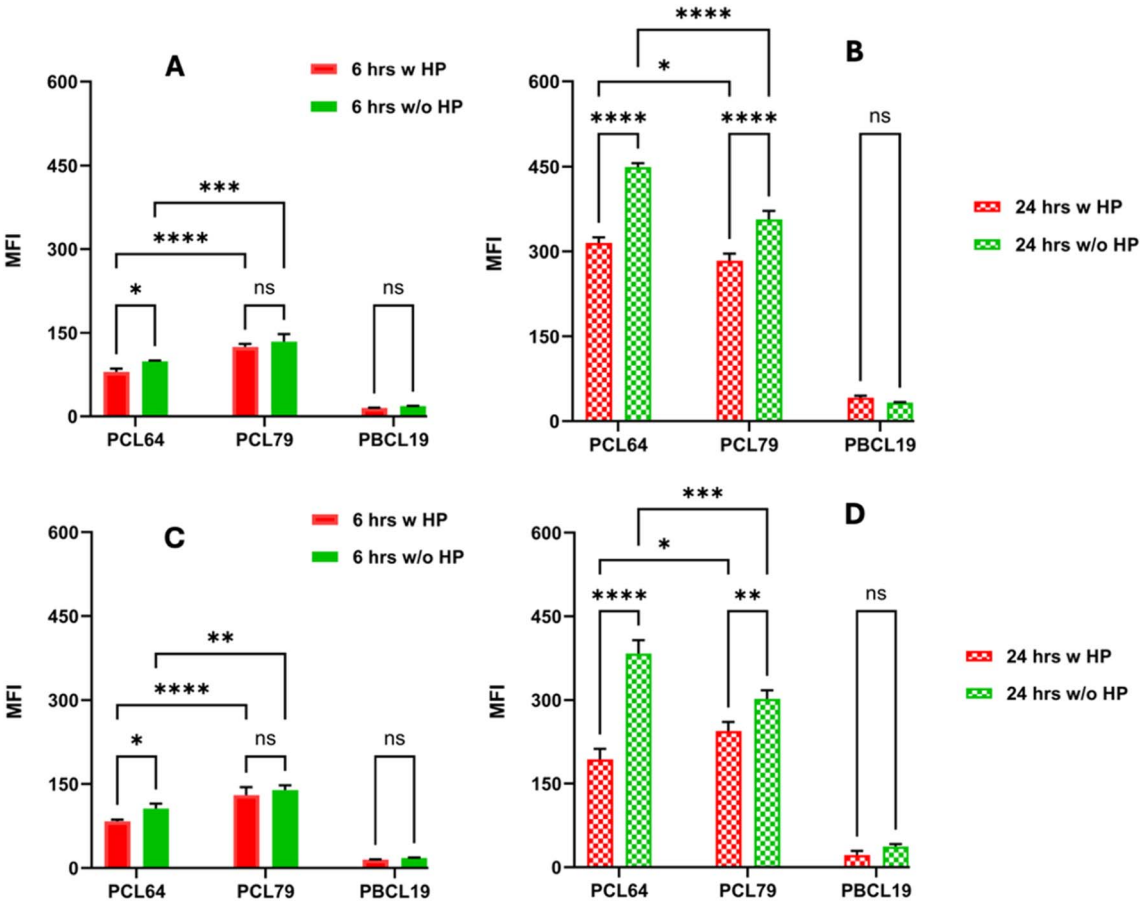

Fig. 3 Uptake of Cy5.5-labelled PEO–PCL and PEO–PBCL micelles by HCT116 cells (A and B); SW620 cells (C and D) following 6 h (A and C) and 24 h (B and D) incubation in the presence (red) and absence (green) of human plasma. The solid bars and checkered bars indicate 6 h and 24 h incubation periods, respectively. Data from three independent experiments were compared by two-way ANOVA multiple comparison test following Tukey's method (*$p \leq 0.05$, **$p \leq 0.01$, ***$p \leq 0.001$, ****$p \leq 0.0001$).

human plasma.[43] This density similarity hinders effective separation, as both the PMs and plasma proteins sediment at comparable rates during centrifugation. Moreover, our initial centrifugation attempts resulted in significant aggregation of the PMs, which not only complicates their isolation but also risks contamination with unbound proteins. Aggregation can alter the surface properties of PMs, affecting their subsequent analysis and reliability of results.

To overcome these challenges, we employed asymmetrical flow field-flow fractionation (FFF). This technique allows for gentle and efficient separation of nanoparticles based on their hydrodynamic size without inducing aggregation.[44] FFF not only provided robust analysis of the PMs' colloidal stability but also facilitated the collection of protein corona-coated PMs for detailed protein composition analysis.

After conducting preliminary FFF analysis on various PM samples (Fig. S7 and S8 of the ESI†), we selected three specific micelles—PCL64, PCL79, and PBCL19—for in-depth protein corona studies. These micelles were chosen primarily because they exhibited a consistent spherical morphology, as confirmed by TEM images presented in Fig. 1. Other samples were excluded because they either formed aggregates or displayed random coil shapes during analysis, making them unsuitable for accurate protein corona characterization due to potential inconsistencies in surface area and protein binding sites.

Fig. 4 illustrates the elution profiles of both bare PMs (left panels) and protein corona-coated PMs (right panels). Notably, the elution times differed between the bare and coated PMs, indicating an increase in hydrodynamic size due to the adsorption of proteins onto the PM surface.

To further elucidate the composition of the protein corona, we selected representative fractions from the initial, middle, and final elution times for LC-MS analysis (see Fig. S7 and S8†). The results, summarized in Fig. 5, revealed distinct protein patterns across the fractions. The middle fractions—associated with the protein corona-coated PMs—displayed remarkably similar heatmaps among the three samples, suggesting a consistent and reproducible protein corona formation. Detailed protein and peptide clusters identified in these middle fractions are provided in the ESI Excel files 1 and 2.† In contrast, the initial fractions showed protein profiles indicative of excess unbound plasma proteins, while the final fractions likely contained aggregates or larger protein–PM complexes, as evidenced by their divergent heatmaps.

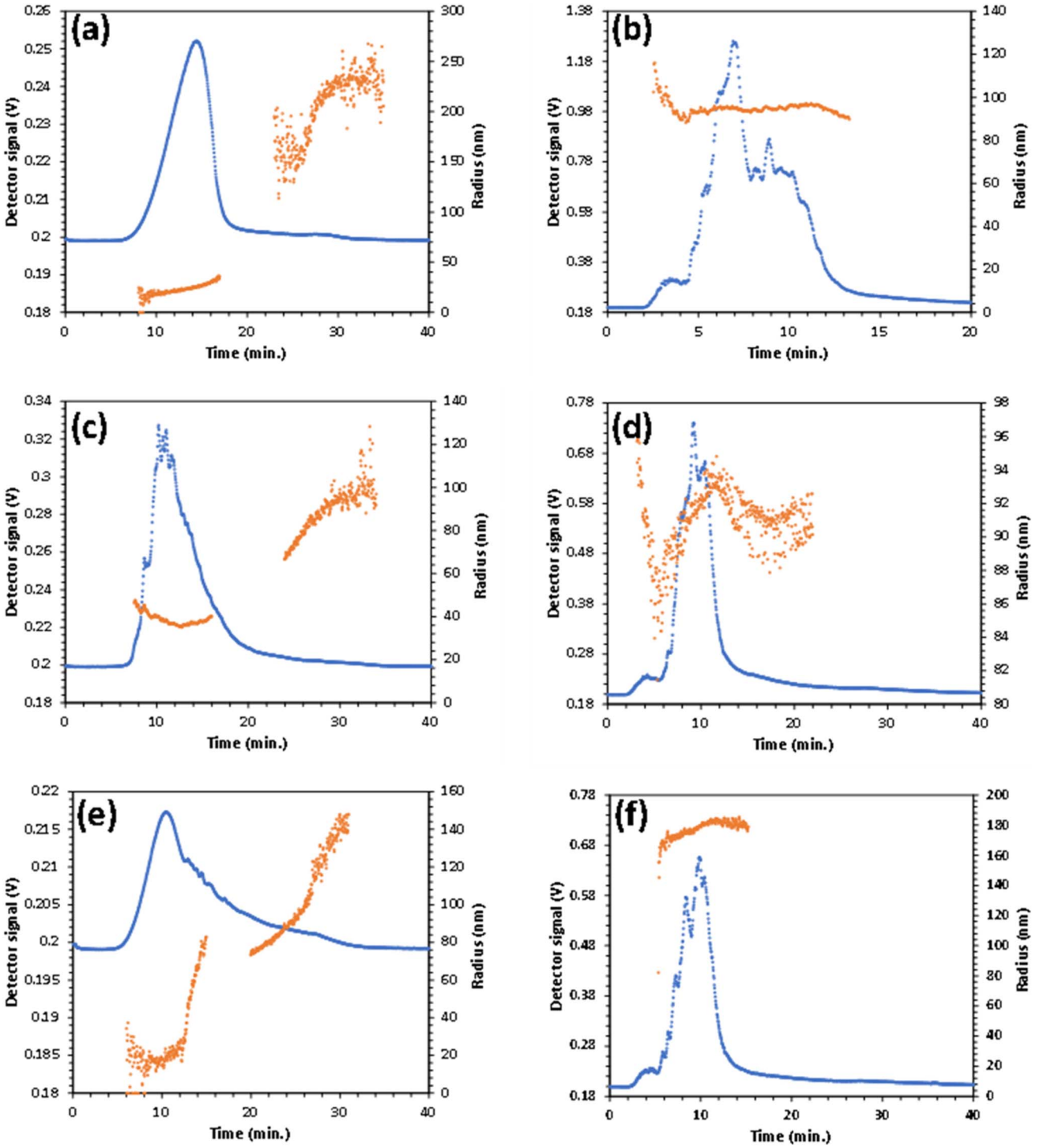

Fig. 4 The FFF histograms of bare NPs (a) PCL64, (c) PCL79, (e) PBCL19, and mixture of NPs incubated with human plasma after injection into the FFF over time (b) PCL64, (d) PCL79, and (f) PBCL19, respectively. Blue dots correspond to the FFF detector signal on left *Y* axis with the retention time on *X* axis, of bare and protein corona-coated micelle, and orange dots corresponds to the right *Y* axis and indicate the mean radius of the bare micelles and protein corona-coated micelle.

Our results demonstrated the efficacy of FFF in isolating and analysing protein corona-coated PMs without inducing aggregation or contamination. By carefully selecting fractions based on elution times, we ensured the analysis focused on monodisperse, spherical PMs with well-defined protein coronas. This approach allowed us to obtain detailed insights into the protein composition of the corona, which is crucial for understanding the biological interactions and fate of PMs in physiological environments.

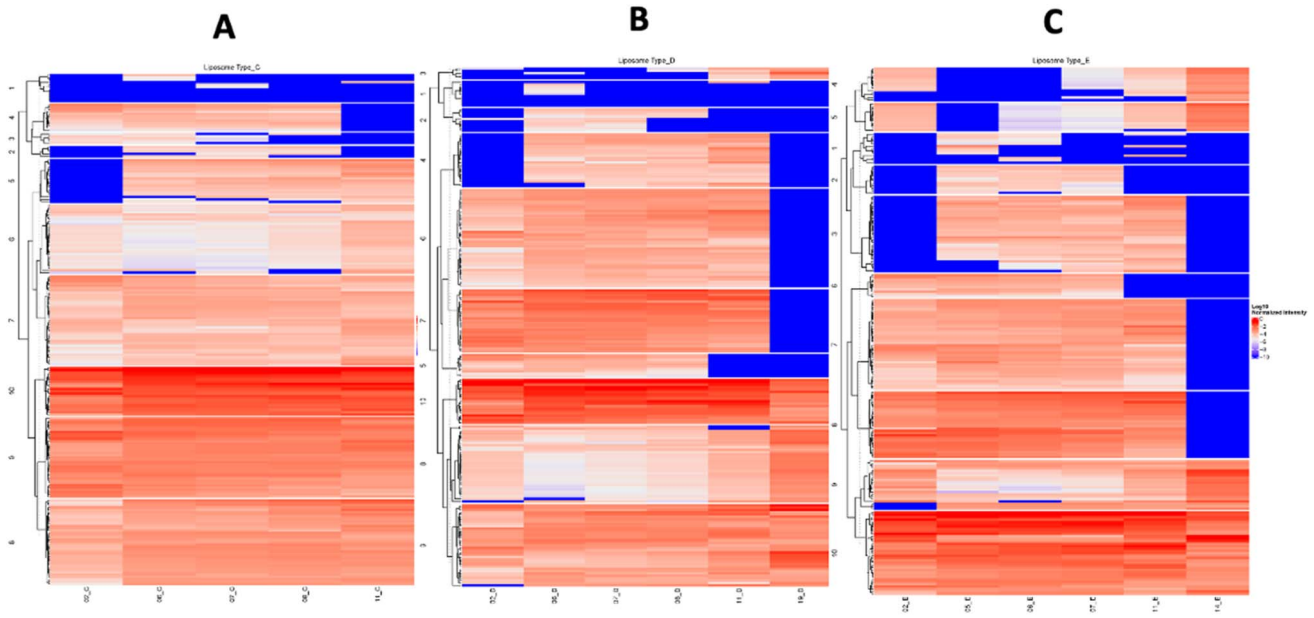

Fig. 5 The hierarchical clustering of (A) PEO–PCL64, (B) PEO–PCL79 and (C) PEO–PBCL19 micelles based on the average abundances of quantified proteins at various elution times and from different fractions (raw data is available in ESI Excel files 3 and 4†).

We then performed a deeper analysis of proteins coronas in the averaged middle fractions. Among the top 20 most abundant proteins for each NP type, 18 proteins were shared, while a few proteins were specific to one or two PMs (Fig. 6A). For example, SERPING1 was only found among the top 20 proteins in the PBCL19 corona. The 20 top proteins from the three PM coronas comprised of 23 unique proteins, which mapped to complement and coagulation pathways and cholesterol metabolism (Fig. 6B) (some of the proteins were immunoglobulins and were not recognized by String DB pathway analysis tool). In Fig. 6C, we visualize the top 10 most abundant proteins found on the surface of each PM, where PCL64 and PCL79 NPs corona had all the top 10 most abundant proteins identical. But two of these proteins, FGB and APOB, were absent in the PBCL19 corona, Instead, two unique proteins, IGHG3 and IGKC, that were not present in the PEO–PCL micelle coronas, were found in the PBCL19 corona.

Orthogonal Partial Least Squares discriminant analysis (OPLS-DA), which is a supervised multivariate data analysis algorithm, was used to identify variables (here, proteins) that differentiate between two groups (in this case, the corona proteomes of different NP types). OPLS-DA can, therefore, highlight the proteins with the largest discriminatory power between the two groups. A detailed description of OPLS-DA can be found in our previous work, where we used OPLS-DA to identify drug targets, enzyme substrates and disease biomarkers.[45–47] We built OPLS-DA models separating each NP corona proteome from others and highlighted the proteins most specifically enriched or depleted in each micelle corona (Fig. 7). On these plots, the blue circles represent reference points for the samples and each green circle is a protein. The proteins closest to the model extremities along the horizontal axis or pq[1] have the largest discriminatory power. While the proteins on the furthest right are those specifically enriched on the corona of the given NP type, those on the furthest left are proteins that are specifically depleted for the given NP type, or simply enriched to a higher level for the other two types. Each OPLS-DA model is characterized by an R^2 value reflecting the goodness of the model fit and a Q^2 value, which represents the predictive power of the model.[48] The Q^2 was only decent for PBCL19, which is probably due to the high similarity that is noted for PCL64 and PCL79 in Fig. 7 (the model is not capable of differentiating highly similar samples). Collectively, the OPLS-DA models revealed the specific enrichment or depletion of several proteins in the corona layer of different PMs. For example, APOA4 and CFI were enriched in the corona of PBCL19 *vs.* corona layers of PCL64 and PCL79, while RPL9 and ACTB were depleted.

Discussion

This study investigated PMs made from seven block copolymers containing hydrophilic shell-forming PEO blocks (DP 114, MW 5000 Da) and PCL or PBCL hydrophobic core-forming blocks of different degrees of polymerization (DPs). Since the hydrophilic PEO block lengths were constant across all polymers, a decrease in size with increasing MW of PCL-containing polymers (as reported in Table 1) could be attributed to the increased compactness and rigidity of the micelles resulting from longer hydrophobic blocks. The longer hydrophobic chain may be thermodynamically more conducive for forming smaller micelles. This is also consistent with previously reported observations,[49] that is, given a fixed hydrophilic block length, a larger hydrophobic length suggests increased polymer hydrophobicity. This promotes a preferred polymer–polymer interaction and tightly compacted aggregate of smaller size.[50]

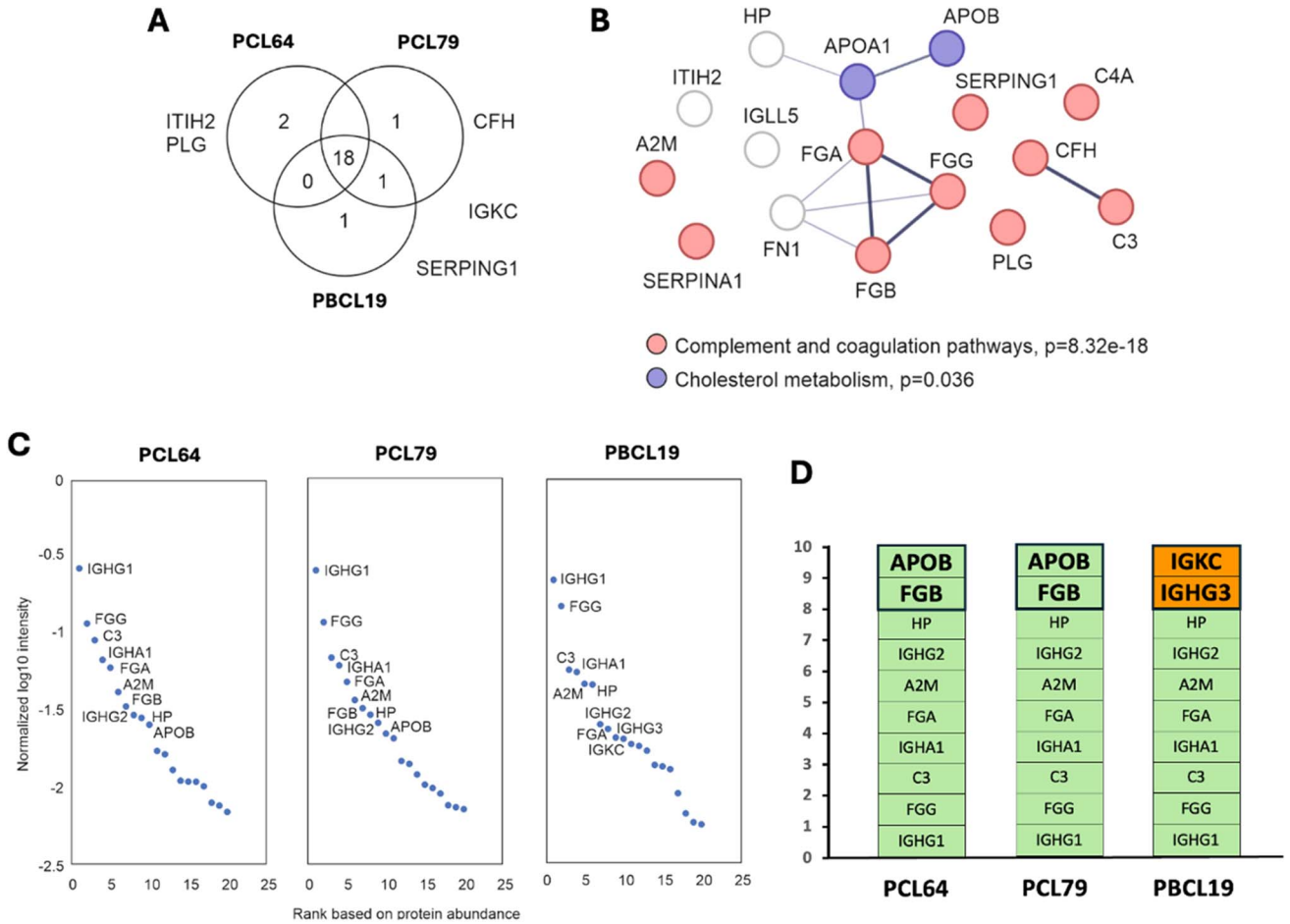

Fig. 6 (A) Venn diagram showing proteins common and unique among the top 20 most abundant proteins in NP coronas. (B) KEGG pathways enriched for the top 23 unique most abundant proteins found in the corona of three NP types. (C) The top 10 most abundant proteins for each NP corona are shown in the order of abundance in LC-MS analysis, (D) variation of proteins among the top 10 most abundant proteins isolated from the corona of three NP types.

The zeta potential values reported in Table 1, revealed that as the DP increases for specific hydrophobic block-containing (PCL or PBCL) PMs, zeta potential becomes more negative. This relationship between DP and zeta potential was found to be significant ($*p < 0.05$, Fig. S2(A) and (B)†). The absolute zeta potential values were lowest for both polymers with DP 19 (PCL19 and PBCL19), likely due to the relatively weaker stability of these two PMs resulted from their smaller hydrophobic blocks. It is well-known that amphiphilic block copolymers with smaller hydrophobic blocks relative to their hydrophilic counterparts result in reduced overall hydrophobicity, which leads to the formation of less stable micelles.[51,52] The increase in zeta potential with longer hydrophobic blocks may reflect the formation of more compact PMs, driven by stronger hydrophobic interactions. The dispersity measured by GPC also decreases significantly as the DP of the PBCL blocks increases. PBCL-containing polymers with DP 19 showed the highest dispersity in the GPC chromatograms (Table 1) and the lowest colloidal stability in FFF fractograms (Fig. 4). Higher dispersity often implies incomplete polymerization or branching, potentially resulting in unexpected behavior of the polymer nanoparticles.

PEG fractions (f_{EO}) are calculated as the ratio of the mass or weight of PEG blocks (MW_{PEO}) to the mass or weight of the entire molecule (MW_{entire}). The rod-like or cylindrical morphologies for PMs with comparatively higher f_{EO} observed in TEM images (Fig. 1) are uncommon, according to many published research findings.[53–56] For example, Lee *et al.*[53] reported that spherical micelles are dominant when the hydrophilic f_{EO} exceeds 0.55. When $0.45 < f_{EO} < 0.50$, cylindrical or worm-like micelles are more likely to form. In another study by Won *et al.*,[57] the observation of worm-like micelles for f_{EO} between 0.47 and 0.59 was reported. In our study, we observed worm-like or rod-like morphologies for f_{EO} 0.7 and 0.5 for PCL-containing micelles. However, Sun *et al.* offered a compelling explanation for the observation of this unusual morphology, suggesting that hydrogen bonding between the hydrophilic block and the hydrophobic segments could promote the formation of cylindrical and rod-like structures in micelles with lower molecular weight core-forming blocks (Fig. 1(A) and (B)).[58] The enhanced hydrophobic interactions of longer hydrophobic

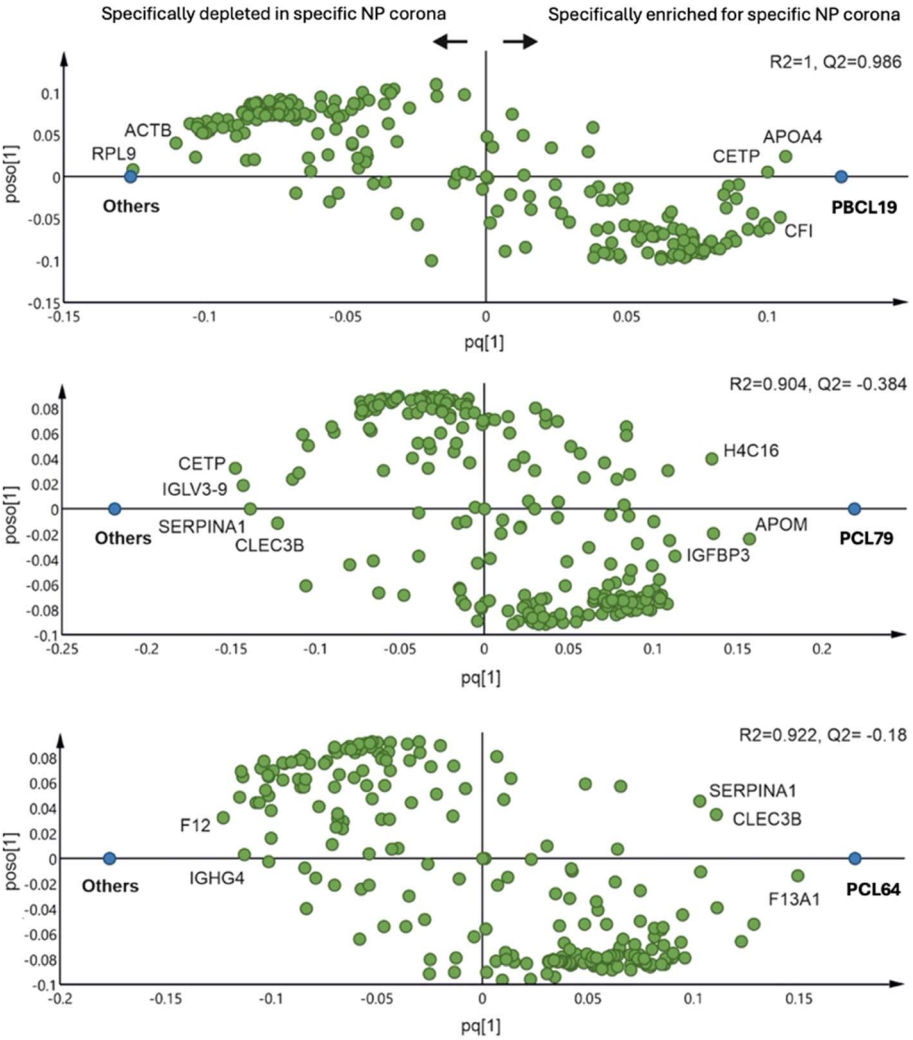

Fig. 7 OPLS-DA models highlighting the enriched and depleted proteins in nanoparticles' protein corona.

blocks could drive the copolymers to minimize their exposure to water, forming more spherical micelles[49] (Fig. 1(C)–(G)).

The lower size measured by TEM compared to DLS is due to the acquirement of TEM images in a dry state, while DLS measures the particles in a hydrated state in aqueous solutions.[59] Besides, DLS is extremely sensitive to large particles and aggregates due to its intensity-weighted measurement, which can significantly distort the size distribution if even a few larger particles are present.[60] This can be another reason for observing larger sizes for DLS than TEM (reported in Table 1).

Although both PCL19 and PCL43 micelles exhibit rod-like morphology, their PDI values differ, likely reflecting variations in morphological uniformity, as observed in the TEM images. PCL19 predominantly formed rod-like structures, whereas PCL43 displayed a mixture of spherical and rod-like morphologies (Fig. 2A and B). This heterogeneous morphology may account for the higher PDI observed in PCL43. Similar findings were reported by Nishimura *et al.*, where larger rod-like nanoparticles (37 nm) exhibited a lower PDI (0.18) compared to smaller spherical particles (19 nm) with a higher PDI (0.27).[61]

In our preliminary study in the presence of FBS, we have seen a lower cellular uptake by PEO–PBCL micelles compared to PEO–PCL micelles, which could reflect a more effective steric barrier against uptake of PEO–PBCL micelles by CRC cells. In general, for PEO–PCL micelles, no significant correlation between the DP of the PCL core and cell uptake was observed. Although the overall cellular uptake for PEO–PBCL micelles was quite low, uptake decreased as the DP of the PBCL block increased, possibly due to the formation of more compact micelles, making the steric barrier on the PBCL micelles more effective. However, we acknowledge that it is an observation specific to a limited number of polymers investigated here and the conclusions made cannot be generalized. Some researchers suggest that hydrophobicity has a significant impact on protein adsorption, potentially exerting a more substantial influence than charge.[17] The adsorption of proteins may increase with the length of the hydrophobic PBCL segment, which acts as a steric barrier in cellular internalization; this observation was also reported by Li *et al.*[30]

The higher cellular uptake of PMs by the HCT116 cell lines compared to the SW620 cell line observed in the *in vitro* cellular uptake study in the FBS-containing media (Fig. 2), is likely due to the metabolic differences and distinct endocytic pathways in the two cell lines. For example, a recent study reported that HCT116 cells can internalize certain nanotubes *via* dynamin-dependent pathways, while SW480 cells (a tumor line from which the metastatic SW620 is derived) may use both dynamin- and clathrin-dependent pathways.[62] Besides, HCT116 cells may uptake more nanoparticles during the cell division process, owing to their faster proliferation rate. Such differences in the primary internalization pathways or the phase of the cell cycle could lead to different uptake rates between SW620 and HCT116 cells.[62]

Taking all data together, it can be stated that PCL19 did not behave in line with other PMs. Both DLS and FFF (Fig. S7(A) of ESI†) exhibited significantly larger sizes, with FFF indicating the formation of large aggregates and reduced colloidal stability compared to other polymers. TEM analysis further revealed unusual worm-like or rod-like morphologies for PCL19 micelles. The DLS can most accurately measure the hydrodynamic diameter of particles with a perfect spherical shape.[63] The presence of non-spherical, morphologies can result in measurement artifacts, potentially causing deviations from the actual particle diameter.

The PCL19 micelles also showed significantly higher cellular uptake, which may be attributed to the rod-like morphology that is preferentially internalized by cells compared to spherical structures.[64] The shift from spherical to rod-like micelles occurs due to reduced stabilization from the hydrophilic segment, causing the original spheres to fuse.[58] The appearance of rod-like structures, even at such a low DP for the hydrophobic block, suggests that the PCL19 provides weak stabilization as a core-forming block. Besides, the less stable PCL19 micelle may dissociate early into their constituent block copolymers, which could be more readily taken up by the cells, resulting in higher fluorescence intensities observed in both cell lines (Fig. 2). The slightly reduced stability of conjugated Cy5.5 and its leakage, as demonstrated in the 24 hour stability study in Fig. S5(A),† may have contributed to the observed higher median fluorescence intensity (MFI) values for PCL19 micelles compared to other PMs in the 24 hour uptake but cannot explain the higher MFI seen at 6 h time point (Fig. 2B and D).

The slightly reduced uptake of PEO–PCL micelles by CRC cells following 24 hour incubation with human plasma compared to plasma free media (Fig. 3B and D) is likely due to the higher protein adsorption that occurs during 24 hour exposure, which provides a steric barrier against cellular internalization. This finding also agrees with previous results that the cell uptake of nanoparticles in serum-free conditions is higher than that seen for the same nanoparticles in serum-containing media.[22]

The chemistry and DP of the polymer core-forming blocks as well as the physicochemical properties of the PMs, contribute to distinct protein corona compositions, which may additionally explain the variation observed in cellular uptake. Studies have highlighted that specific proteins constituting the corona can interact with specific cell receptors, potentially guiding the nanoparticles to their target cells. For example, apolipoproteins such as ApoH, ApoA4, and ApoC3 have been identified as key regulators of nanoparticle uptake in human mesenchymal stem cells.[65] Among the top 20 most abundant proteins analyzed from the PMs' protein corona under study (Fig. 6A), ITIH2, PLG, and CFH proteins isolated from PCL64 (zeta potential $= -16.4 \pm 1$) and PCL 79 ($ZP = -21.1 \pm 0.4$) are more likely to have a higher tendency to adsorb to negative zeta potential surfaces than SERPING1 found in PBCL19 ($ZP = -5.4 \pm 0.1$). The relatively less negative surface zeta potential of PBCL19 micelles compared to the PCL micelles, as reported in Table 1, can explain this variability in the protein corona observed. PLG (plasminogen) has regions with positive charges, particularly in its kringle domains, known for their high affinity for lysine residues, which could facilitate binding to negatively charged surfaces. Fibrinogen (FGB) and APOB (apolipoprotein B) were identified in the top 10 most abundant proteins isolated from PCL64 and PCL79 corona but not in the PBCL19 corona (Fig. 6C and D). The inclusion of FGB and APOB in the protein corona of PCL64 and PCL79 PMs may significantly enhance their interactions with immune cells by engaging specific receptors and uptake pathways. FGB and APOB have a relatively higher tendency to attach to negative surfaces than IGHG3 and IGKC.[13]

Besides, previous studies show that apolipoproteins have a higher affinity for more hydrophobic materials, which can explain their absence in the top 10 most abundant proteins isolated from PBCL19 corona (less hydrophobic compared to PCL64 and PCL79).[66] FGB is known to bind to integrin receptors on the surface of various cell types, including immune cells.[13] When fibrinogen is part of the NPs' protein corona, it can mediate binding to these integrin receptors,[13] facilitating enhanced cellular adhesion and uptake of the NPs. The presence of FGB on PM corona layer can promote interaction of their binding sites with integrins on cell surfaces, which might trigger cellular uptake pathways such as endocytosis and facilitate further internalization. APOB is a primary component of low-density lipoproteins (LDL)[67] and is recognized by LDL receptors on the surface of many cell types, including liver cells and some cancer cells. Nanoparticles with APOB in their protein corona can mimic LDL particles, promoting uptake *via* receptor-mediated endocytosis through LDL receptors.

While the inherent physicochemical properties of the polymeric micelles are primary determinants of cellular uptake, the composition of the adsorbed protein corona—particularly the enrichment of fibrinogen (FGB) and apolipoprotein B (APOB) on the PCL micelles in this study—can further modulate these nanoparticle–cell interactions following plasma exposure. The presence of specific proteins like FGB and APOB in the corona may introduce additional mechanisms for cellular association and internalization, for instance, by engaging cell surface receptors such as integrins or LDL receptors, respectively, thereby influencing the overall uptake profile. It is important to emphasize that these corona components are not proposed as the sole determinants of the observed differences in cellular uptake. Rather, it is more likely that specific adsorbed proteins, such as FGB and APOB, together with the intrinsic

physicochemical attributes of the PEO–PCL micelles, potentially synergistically influenced cellular internalization. Nevertheless, in the context of CRC cells understudy, the presence of FGB and APOB in the protein corona composition of PEO–PCL micelles, seemed to have a negative effect reducing the uptake and internalization of these nanocarriers by the target cells. We acknowledge that a more extensive analysis, incorporating a broader range of PEO–PBCL (and PEO–PCL) micelles could strengthen our conclusions, and we plan to incorporate broader datasets in future studies to better delineate the relative contributions of corona composition and intrinsic physicochemical properties.

Experimental

Materials

Methoxy-polyethylene oxide (PEO) (average molecular weight of 5000 g mol^{-1}) and ε-caprolactone were purchased from Sigma (St. Louis, MO) and extra purified in-house by vacuum distillation. α-Benzyl carboxylate-ε-caprolactone and α-propargyl carboxylate-ε-caprolactone monomers were synthesized by Alberta Research Chemicals Inc. (Edmonton, Canada) according to a previously published procedure.[38,68,69] Stannous octoate was purchased from MP Biomedicals Inc. (Tuttlingen, Germany) and purified by vacuum distillation. Copper(II)–TBTA complex and Cy5.5-azide were acquired from Lumiprobe (Hallandale Beach, FL, USA). Cell culture media DMEM, fetal bovine serum (FBS), and penicillin–streptomycin-L-glutamine were purchased from GIBCO, Life Technologies Inc. (Burlington, ON, Canada). Spectra/Por dialysis tubing (MWCO, 1 kDa and 3.5 kDa) was purchased from Spectrum Laboratories (Rancho Dominguez, CA). All other chemicals were reagent grade. Costar black polystyrene round bottom 96-well plates were obtained from Corning Inc (Kennebunk, ME), and TC sterile 6-well plates were purchased from Sarsted (Germany). HCT116 (CCL-247) and SW620 (CCL-227) cells were obtained from American Type Culture Collection (ATCC). Pooled healthy human plasma was purchased from Innovative Research (Novi MI, USA, Cat# IPLAWBK2E50 ML). Protein physicochemical properties (*e.g.* theoretical isoelectric points (pI)) were calculated using the ExPASy Compute pI/Mw tool [(**https://web.expasy.org/protparam/**) Swiss Institute of Bioinformatics], which computes the pI based on the protein's primary sequence obtained from Uniprot (**https://www.uniprot.org/**).

Synthesis of PEO–PCL and PEO–PBCL di-block copolymers

Block copolymers of PEO-*b*-PCL and PEO-*b*-PBCL of different degrees of polymerization were synthesized by ring-opening polymerization using methoxy-PEO (MW: 5000 g mol^{-1}) and ε-caprolactone (0.5 g, 1 g, 1.5 g, and 1.8 g with 1 g of methoxy-PEO) or α-benzyl carboxylate-ε-caprolactone (1 g, 1.7 g, and 3 g with 1 g of methoxy-PEO), respectively, and stannous octoate as a catalyst.[70,71] Briefly, methoxy-PEO (5 g), ε-caprolactone or α-benzyl carboxylate-ε-caprolactone, and stannous octoate were added to a previously flamed 10 mL ampoule, which was then nitrogen purged and vacuum sealed. The polymerization reaction was allowed to proceed for 4 h at 140 °C in the oven. The reaction was terminated by cooling the product to room temperature. Different ε-caprolactone and α-benzyl carboxylate-ε-caprolactone monomer to methoxy PEO feed ratios were used to prepare PEO-*b*-PCL and PEO-*b*-PBCL block copolymers with varying degrees of ε-caprolactone polymerization. The reaction product was dissolved in DCM, precipitated, and washed with an excess of cold hexane and collected after centrifugation, and dried under vacuum for 48 h.

Attachment of PCC block to the di-block copolymers

Block copolymers of PEO–PCL or PEO–PBCL were end-capped with α-propargyl carboxylate-ε-caprolactone (PCC) using stannous octoate as catalyst. Briefly, PEO–PCL (0.1 mmol) and PCC (0.5 mmol) were added to a 25 mL round-bottom flask filled with 5 mL dry toluene under constant stirring. Stannous octoate (0.010 equiv. of monomer) was added to the flask. The flask was then refluxed for 36 h. The reaction was terminated by cooling the product to room temperature. The product was then precipitated in hexane and the supernatant was discarded. The final product was washed with ether, followed by centrifuge collection and dried under vacuum for further use.

Characterization of the synthesized block copolymers

After the ring-opening polymerization reaction between methoxy-PEO and either ε-caprolactone (CL) or α-benzyl carboxylate-ε-caprolactone (BCL) monomers, the number-average molecular weights of the diblock copolymers (PEO–PCL, PEO–PBCL) and the triblock copolymers (PEO–PCL–PCC, PEO–PBCL–PCC) were determined using ^{1}H NMR (Bruker Avance III spectrometer, Bruker BioSpin Corporation, Billerica, MA), according to previously published methods.[70,71] The DP of PCL or PBCL was determined by comparing the peak intensity of PEO hydrogens (–CH_2CH_2O–, d = 3.65 ppm) to the intensity of the peak for methylene hydrogen (–OCH_2–, d = 4.05 ppm), corresponding to PCL or PBCL backbone considering a 5000 g mol^{-1} molecular weight for PEO.

The number-average molecular weight of PEO–PCL–PCC and PEO–PBCL–PCC tri-block copolymers after end-capping with α-propargyl carboxylate-ε-caprolactone (PCC) was determined from the ^{1}H NMR spectrum of the block copolymers in $CDCl_3$ at 600 MHz by comparing the peak intensity of the hydrogens of PEO (–CH_2CH_2O–, δ = 3.65 ppm) to the methylene hydrogens of PCC block (–OCH_2–, δ = 4.75 ppm), considering a 5000 g mol^{-1} molecular weight for PEO.

The number average molecular weight (M_n) and dispersity ($Đ$) of the synthesized polymers were analyzed by gel permeation chromatography (GPC). Samples were dissolved in THF (~5 mg mL^{-1}), filtered through (0.22 μm), and manually injected in an Agilent 1260 infinity system equipped with two Waters columns (Strygel HR2 and Strygel HR4E). The flow rate of 0.7 mL min^{-1} and the volume of injection was 100 μL. Molecular weight was calculated based on a calibration curve prepared using polystyrene standards (MW 3.7, 9.9, 13.0, 21.0, 44.0, and 76.0 kDa). The concentration *versus* elution time data was then integrated and analyzed to calculate the weight-average

molecular weight (M_w), the number-average molecular weight (M_n), and the dispersity ($Đ = M_w/M_n$).

Conjugation of NIRF Cy5.5 to the tri-block copolymers

Near-infrared fluorophore (NIRF) Cy5.5-azide, purchased from Lumiprobe, was conjugated to the terminal alkyne of PCC in PEO–PCL–PCC or PEO–PBCL–PCC using Huisgens 1,3-dipolar cycloaddition (azide–alkyne click chemistry) reaction. The terminal alkyne group of PCC reacted with the terminal azide group of Cy5.5 azide to form a 1,3-triazole ring.[33] Cu(I) acts as a catalyst for the reaction. Cu(I) is prepared *in situ* by the addition of Cu(II) TBTA complex, and ascorbic acid, reducing Cu(II) to Cu(I). Briefly, 10 μmol PEO–PCL–PCC or PEO–PBCL–PCC (75 mg) was dissolved under constant stirring in a 10 mL round-bottom flask containing 2 mL degassed DMSO. Cy5.5 azide (1 μmol; 0.7 mg) was dissolved in 400 μL DMSO and added to the mixture under constant stirring followed by addition of ascorbic acid (0.5 μmol; 0.1 mg) previously dissolved in 100 μL water. The flask was then degassed with argon for about 30 s. 10 mM Cu–TBTA Complex solution (0.5 μmol; 60 μL) was finally added followed by degassing for 30 s using argon. The reaction mixture was sealed and incubated with stirring at room temperature in the dark for 16 h. Argon was flushed through the sealed vial at 4 and 8 h time-points. After incubation, the mixture was separated from the non-reacted dye by dialysis (MWCO 1 kDa) against DMSO for 24 h followed by dialysis against water for 24 h to remove the DMSO, and then lyophilized.

Specific quantities of the polymers were dissolved in DMSO and analyzed at 700 nm emission wavelength using 670 nm excitation wavelenght in a BioTek plate reader to measure Cy5.5 fluorescence intensity. Cy5.5 concentrations in each polymer sample were calculated from the standard Cy5.5 calibration curve. The conjugation efficiency for each polymer was calculated as the percent of ratio of the quantity of Cy5.5 present in the total polymer after the click reaction and the quantity of Cy5.5 added to the reaction mixture.

Formulation and characterization of PMs

PEO–PCL or PEO–PBCL block copolymer micelles, with or without Cy5.5, were prepared through cosolvent evaporation as described before.[69] For Cy5.5 labelled micelles, the formation of mixed micelles from blank copolymers and Cy5.5 conjugated polymer was used, as detailed in Table S1.† Each well containing CRC cells was to be treated with 50 nmol of total polymer containing 0.3 μg of Cy5.5. For that, the ratio of Cy5.5-conjugated polymer and non-conjugated polymer in the final mixed micelle was calculated based on the different conjugation efficiencies of different polymers. Briefly, calculated quantities of Cy5.5-conjugated and non-conjugated polymer were dissolved in acetone (0.6 mL). The solution was added to deionized water in a drop-wise manner under moderate stirring at room temperature, followed by evaporating acetone under vacuum overnight. The prepared micellar solution was then centrifuged to remove any aggregates. The average size and size distribution of micelles were measured by dynamic light scattering (DLS) at backscatter angle 173° using Zetasizer Ultra (Malvern Panalytical, Worcestershire, UK). The Cy5.5 concentration in each micelle solution was measured in a BioTek plate reader as described in Section 1.5 above. A required volume of 10× PBS was added to make the final concentration of the solution to 1× PBS. Further dilution was made so that a specific volume of polymeric micelle solution will contain 50 nmol of total polymer and 0.3 μg Cy5.5.

Morphology investigation by transmission electrone microscopy (TEM) imaging

The morphology of polymeric micelles was studied by TEM. A small drop of micellar dispersion (polymer concentration of 1 mg mL^{-1}) was deposited on a copper-coated grid, allowed to settle at room temperature for 2 minutes and dried using Whatman filter paper. After that, the samples were stained with 1% uranyl acetate solution, which was also removed right away using filter paper followed by air drying. Then, samples were analyzed in a Morgagni 268 TEM microscope (Philips/field emission) operated at 80 kV and image acquisition was performed using a Gatan Orius CCD camera. The TEM images were analyzed using ImageJ software (**http://imagej.org**, Java1.8.0_345). Diameters or width of particles were measured for spherical and rod-shaped morphologies, respectively.

Assessing the *in vitro* stability of the Cy5.5-conjugated micelles

The *in vitro* release of Cy5.5 dye was studied using the equilibrium dialysis method to check if Cy5.5 is released from the polymer after preparing the polymeric micelles. Polymeric micelle dispersions were prepared by cosolvent evaporation as described before.[69] 10× PBS was added to make them 10% PBS-containing micelle dispersions. Dialysis tubing (MWCO 3500 Da) was prepared containing 4 mL of each micelle dispersion (conc. 0.5 mg mL^{-1}). The release study was carried out at 37 °C for 24 h in 300 mL of PBS and DMEM media to ensure sink conditions and under shaking at 65 rpm in a water bath system (Julabo SW 22, Seelbach, Germany). After 24 h, aliquots of 200 μL were collected from inside the dialysis bags. Fluorescence was measured at 700 nm emission wavelength using 670 nm excitation wavelenght by a BioTek Plate reader and calculated from the standard Cy5.5 calibration curve.

In vitro cellular uptake study in 10% FBS-containing media

HCT116 cells and SW620 cells were grown in DMEM cell culture media containing 10% FBS and penicillin-streptomycin-glutamine. HCT116 cells and SW620 cells were seeded into 6-well plates at densities of 1.2×10^5 cells per well and 1.8×10^5 cells per well, respectively. The plates were incubated at 37 °C for 24 h until 70% confluency was reached. Micelles of PEO–PCL and PEO–PBCL were added to the wells so that each well contains 0.3 μg Cy5.5 by the addition of micelle solution. PBS was used to treat three negative control wells. The plates were incubated for 6 h and 24 h at 37 °C ($n = 3$). After the incubation period, cells were washed three times with PBS and trypsinized. 4% paraformaldehyde in PBS solution was used to fix the cells

and FACS buffer was added. The cells were strained through the cell strainer into Falcon® 12 × 75 mm tube with a 35 μm nylon mesh cell strainer cap. The uptake was analyzed on Attune NXT flow cytometer. 10 000 events were collected for each sample. The data were analyzed with the FlowJo software.

In vitro cellular uptake of PMs in the absence and presence of human plasma

Pooled healthy human plasmas were diluted with phosphate buffer solution (PBS, 1×) to a concentration of 55%. HCT116 cells and SW620 cells in DMEM cell culture media without the presence of FBS were seeded into 6-well plates and incubated following the same conditions as described above. When the cells reached 70% confluency after 24 h incubation, 10% volume of media was discarded and replaced with 10% human plasma (HP). Cy5.5-labeled PCL64, PCL79 and PBCL19 polymeric micelles were added to the wells so that each well contains 0.3 μg Cy5.5 by adding micelle solution. The plates were incubated for 6 h and 24 h at 37 °C ($n = 3$). After the incubation period, the cells were harvested and analysed by flow cytometry, as described above.

Protein corona formation and characterization

For protein corona formation, each PM sample was incubated with 55% human plasma (with PM concentration of 0.2 mg mL^{-1}) for 1 h at 37 °C. To remove unbound and loosely attached plasma proteins from the surface of NPs, the protein–NP mixture was then introduced to field flow fractionation (FFF) instrument and 1 mL elution was collected every one minute for further analysis (Fig. 8).

FFF sample preparation

The three PMs (PCL64, PCL79 and PBCL19) were analyzed using the Postnova Asymmetrical Flow Field-Flow Fractionation (AF4) system with a Multi-Angle Light Scattering (MALS) detector (PN3621), UV/Vis detector (PN3211), Autosampler (PN5300), fraction collector (PN8050), and Refractive Index (RI) detector (PN3150). The carrier solution was a 10× diluted PBS buffer from Sigma. A 150 kDa PES membrane from Postnova Analytics was to filter the excess plasma protein during the separation and collection step. Each sample was injected with a volume of 100 μL, and the channel flow rate was set at 1 mL min^{-1}. The crossflow rate was initially set at 1 mL min^{-1} for 2 min, reduced to 0.1 mL min^{-1} in 25 min, and kept constant at 0.1 mL min^{-1} for the rest of the run. Two replicates were analyzed for each sample. For the incubation study, the NPs were incubated with two plasma samples at 37 °C for 60 min and immediately analyzed by AF4-MALS. 30–32 1 mL fractions were collected during the fractionation. The MALS, UV/Vis, and RI detectors provided data, which was analyzed using the Postnova AF2000 software. The MALS data was used to calculate the size distributions of the samples. The root-mean-square (RMS) radii were calculated using the sphere model.

LC-MS/MS

The selected PMs were incubated with human plasma to allow the formation of a protein corona. Immediately after incubation, the PM-protein mixtures were introduced into the FFF system to separate the protein corona-coated PMs from excess and unbound plasma proteins. During FFF analysis, fractions were collected at one-minute intervals from 2 to 34 minutes and stored at −20 °C for subsequent liquid chromatography-mass spectrometry (LC-MS) analysis. Samples were loaded onto a 12% Bolt™ SDS–PAGE gel (Bis–Tris, 1.0 mm, Mini Protein Gel, 10-well; Thermo Fisher Scientific) and electrophoresed until proteins migrated approximately 1 cm into the gel. The protein-containing gel segment was excised, reduced with dithiothreitol (DTT), and alkylated with iodoacetamide. The gel samples were then washed, destained, and the proteins were digested overnight at 37 °C with 250 ng of sequencing-grade trypsin (Promega, Cat# V5111). Peptides were extracted from the gel pieces, dried, and reconstituted in 30 μL of 5% acetonitrile and 0.5% trifluoroacetic acid. Three injections of 5 μL each were analyzed

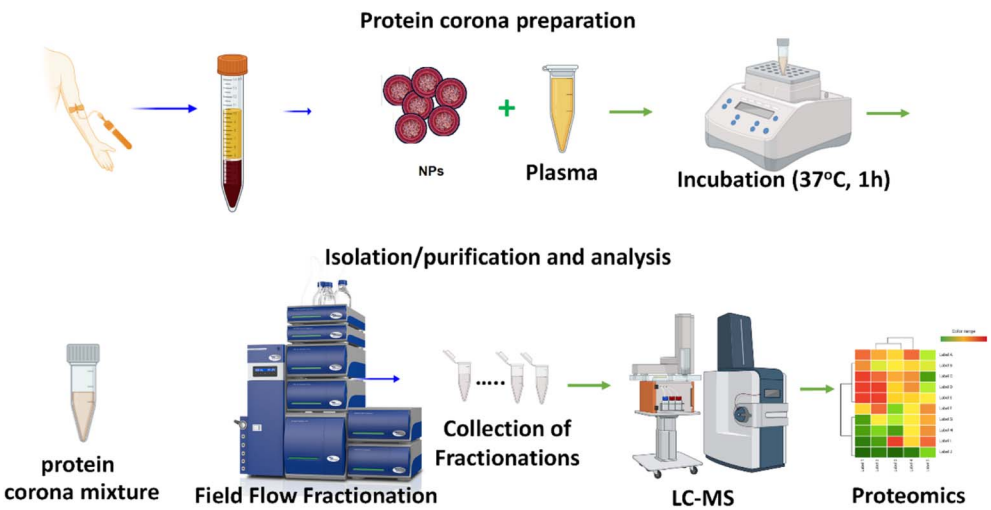

Fig. 8 Schematic workflow for generation and purification of protein coronas on PMs.

by nanoLC-MS/MS using a 2 hour method on a Waters CSH C18 column (0.075 mm × 250 mm; Waters Corporation, Milford, MA), coupled to an Orbitrap Eclipse mass spectrometer (Thermo Fisher Scientific) operating in Orbitrap–Orbitrap (OT–OT) mode.

Proteomics data extraction and processing

Protein quantification was performed using Proteome Discoverer software (Thermo Fisher Scientific, version 2.4). All MS/MS data were searched with Mascot (version 2.7.0; Matrix Science, London, UK), configured to search the cRAP_20150130.fasta database (125 entries) and the UniProt-human_20210508 database (77 027 entries), assuming trypsin digestion. The fragment ion mass tolerance was set to 0.02 Da, and the parent ion tolerance to 10 ppm. Deamidation of asparagine and glutamine, as well as oxidation of methionine, were specified as variable modifications, while carbamidomethylation of cysteine was set as a fixed modification. Peptide identifications were validated using Percolator with a posterior error probability (PEP) threshold of 0.01. A decoy database search was employed to control the false discovery rate (FDR) at 1% (high confidence).

Data analysis

The protein intensities were normalized to the total protein intensity in each sample and were then log10 transformed. Contaminants were removed. For normalization across all samples, the values for missing proteins in each sample before log10 transformation were set to 10^{-10}.

For building the OPLS-DA models, SIMCA 17 was used with default settings (Umetrics).

Network mapping

GO pathway enrichment analysis for the top proteins was performed using the StringDB tool version 11.5.[72]

Statistical analysis

Statistical analysis was performed using two-way ANOVA with Tukey post-test analysis. The significance level (α) was set at 0.05. GraphPad Prism was used (version 10.3, GraphPad Software Inc., La Jolla, CA). All experiments were conducted in triplicate unless mentioned otherwise. In tables or graphs, data points are represented as mean ± standard deviation (SD).

Conclusion

This study provides a comprehensive analysis of how the chemical structure and degree of polymerization (DP) of hydrophobic core-forming blocks in polymeric micelles (PMs) influence protein corona composition and subsequent cellular uptake by colorectal cancer (CRC) cells. We synthesized and characterized seven block copolymers of poly(ethylene oxide)-*block*-poly(ε-caprolactone) (PEO–PCL) and PEO-*block*-poly(α-benzyl carboxylate-ε-caprolactone) (PEO–PBCL) with varying hydrophobic block lengths. The PMs formed from these copolymers displayed sizes ranging from 44 to 99 nm with slightly negative zeta potentials, and their morphology was dependent on the DP of the hydrophobic block. Our findings revealed that PEO–PCL micelles exhibited significantly higher cellular uptake compared to PEO–PBCL micelles in both HCT116 and SW620 CRC cell lines. The presence of human plasma notably reduced the uptake of PEO–PCL micelles but had no significant effect on PEO–PBCL micelles. This suggests that the protein corona formed in human plasma might have played a pivotal role in modulating cellular interactions and internalization of PMs. Proteomic analysis of the protein coronas identified 23 distinct proteins among the top 20 most abundant proteins across all PM types, with 18 proteins common to all micelles. Notably, PEO–PCL micelles shared an identical top 10 protein profile, including fibrinogen (FGB) and apolipoprotein B (APOB), which were absent in the PEO–PBCL micelles. Instead, PEO–PBCL micelles featured two unique proteins, IGHG3 and IGKC. The presence of FGB and APOB in the corona of PEO–PCL micelles may contribute to slightly enhanced interactions with cell surface receptors such as integrins and LDL receptors, facilitating cellular uptake. In contrast, the unique proteins found on PEO–PBCL micelles may not promote such interactions, accounting for their lower uptake. The differential protein adsorption is attributed to variations in surface properties, particularly zeta potential and hydrophobicity, influenced by the DP and chemistry of the hydrophobic blocks. PEO–PCL micelles with longer hydrophobic blocks exhibited more negative zeta potentials and higher hydrophobicity, favouring the adsorption of proteins like FGB and APOB that can enhance cellular uptake in cells overexpressing receptors for these ligands. The less negative zeta potential and lower hydrophobicity of PEO–PBCL micelles may contribute to a protein corona composition that does not facilitate cellular internalization. This study highlights the critical role of protein corona composition in determining the biological identity and fate of nanocarriers. While this study provides valuable insights into how polymer structure, DP, micelle physicochemical properties like size, zeta potential, morphology and hydrophobicity influence protein corona composition and cellular uptake, the proteomic analysis was limited to three polymeric micelles due to experimental constraints related to colloidal stability, morphology, and FFF compatibility. Thus, while informative, the current findings may not fully capture the diversity of corona profiles across all polymeric micelle architectures. Future studies are required to expand this analysis to a broader range of polymeric micelles, including additional PBCL DPs, to further clarify structure–corona–function relationships. Understanding the interplay between polymer structure, protein corona formation, and cellular uptake is essential for the rational design of nanocarriers with optimized therapeutic efficacy. By tailoring the physicochemical properties of PMs, it may be possible to control protein adsorption and, consequently, modulate cellular interactions to enhance targeted drug delivery. Future research should focus on elucidating the mechanistic pathways through which specific corona proteins influence nanoparticle–cell interactions. Additionally, *in vivo* studies are necessary to confirm the translational relevance of these findings and to

assess the impact of protein corona composition on the pharmacokinetics and biodistribution of polymeric micelles. This knowledge will contribute to the development of advanced nanomedicine platforms with improved safety profiles and therapeutic outcomes.

Data availability

The datasets generated during and/or analysed during the current study are available from the corresponding author on reasonable request.

Author contributions

All authors contributed to the study conception and design. Material preparation, data collection and analysis were performed by MS, PP, and SS; characterization of PMs with DLS and zeta potential were performed by AAA; HG and AAS performed proteomics data analysis and visualization; ST performed FFF analysis. The first draft of the manuscript was written by MS. AL and MM commented and edited the versions of the manuscript. All authors read and approved the final manuscript.

Conflicts of interest

Afsaneh Lavasanifar is the co-founder and Chief scientific officer of Meros Polymers, which has the license to PEO-*b*-PBCL polymer used in this manuscript. Morteza Mahmoudi discloses that (i) he is a co-founder and director of the Academic Parity Movement (**www.paritymovement.org**), a non-profit organization dedicated to addressing academic discrimination, violence and incivility; (ii) he is a co-founder of Targets Tip and AlbuDerm; and (iii) he receives royalties/honoraria for his published books, plenary lectures, and licensed patents.

Acknowledgements

This work was supported by a discovery grant (RGPIN-2019-05979) funded by the Natural Science and Engineering Research Council of Canada (NSERC) to A. L. Munira Sirazum acknowledges funding from the PoND training CREATE program from NSERC, and graduate student awards received from Faculty of Pharmacy and Pharmaceutical Sciences, University of Alberta.

References

1 M. Ghezzi, S. Pescina, C. Padula, *et al.*, Polymeric micelles in drug delivery: An insight of the techniques for their characterization and assessment in biorelevant conditions, *J. Controlled Release*, 2021, **332**, 312–336, DOI: **10.1016/j.jconrel.2021.02.031**.

2 K. Kuperkar, D. Patel, L. I. Atanase and P. Bahadur, Amphiphilic Block Copolymers: Their Structures, and Self-Assembly to Polymeric Micelles and Polymersomes as Drug Delivery Vehicles, *Polymers*, 2022, **14**(21), 4702, DOI: **10.3390/polym14214702**.

3 M. Hibino, K. Tanaka, M. Ouchi and T. Terashima, Amphiphilic Random-Block Copolymer Micelles in Water: Precise and Dynamic Self-Assembly Controlled by Random Copolymer Association, *Macromolecules*, 2022, **55**(1), 178–189, DOI: **10.1021/acs.macromol.1c02186**.

4 D. Bobo, K. J. Robinson, J. Islam, K. J. Thurecht and S. R. Corrie, Nanoparticle-Based Medicines: A Review of FDA-Approved Materials and Clinical Trials to Date, *Pharm. Res.*, 2016, **33**(10), 2373–2387, DOI: **10.1007/s11095-016-1958-5**.

5 Y. Zhang, T. Ren, J. Gou, *et al.*, Strategies for improving the payload of small molecular drugs in polymeric micelles, *J. Controlled Release*, 2017, **261**, 352–366, DOI: **10.1016/j.jconrel.2017.01.047**.

6 A. G. Niculescu and A. M. Grumezescu, Polymer-Based Nanosystems—A Versatile Delivery Approach, *Materials*, 2021, **14**(22), 6812, DOI: **10.3390/ma14226812**.

7 T. Cedervall, I. Lynch, S. Lindman, *et al.*, Understanding the nanoparticle–protein corona using methods to quantify exchange rates and affinities of proteins for nanoparticles, *Proc. Natl. Acad. Sci. U. S. A.*, 2007, **104**(7), 2050–2055, DOI: **10.1073/pnas.0608582104**.

8 D. Walczyk, F. B. Bombelli, M. P. Monopoli, I. Lynch and K. A. Dawson, What the Cell "Sees" in Bionanoscience, *J. Am. Chem. Soc.*, 2010, **132**(16), 5761–5768, DOI: **10.1021/ja910675v**.

9 S. Tenzer, D. Docter, J. Kuharev, A. Musyanovych, V. Fetz, R. Hecht, F. Schlenk, D. Fischer, K. Kiouptsi, C. Reinhardt, K. Landfester, H. Schild, M. Maskos, S. K. Knauer, R. H. Stauber, Rapid Formation of Plasma Protein Corona Critically Affects Nanoparticle Pathophysiology, in *Nano-Enabled Medical Applications*, Jenny Stanford Publishing, 2020, pp. 251–278, DOI: **10.1201/9780429399039-9**.

10 L. Vroman, A. Adams, G. Fischer and P. Munoz, Interaction of high molecular weight kininogen, factor XII, and fibrinogen in plasma at interfaces, *Blood*, 1980, **55**(1), 156–159, DOI: **10.1182/blood.V55.1.156.156**.

11 H. Noh and E. A. Vogler, Volumetric interpretation of protein adsorption: Competition from mixtures and the Vroman effect, *Biomaterials*, 2007, **28**(3), 405–422, DOI: **10.1016/j.biomaterials.2006.09.006**.

12 M. Lundqvist, J. Stigler, G. Elia, I. Lynch, T. Cedervall and K. A. Dawson, Nanoparticle size and surface properties determine the protein corona with possible implications for biological impacts, *Proc. Natl. Acad. Sci. U. S. A.*, 2008, **105**(38), 14265–14270, DOI: **10.1073/pnas.0805135105**.

13 Z. J. Deng, M. Liang, M. Monteiro, I. Toth and R. F. Minchin, Nanoparticle-induced unfolding of fibrinogen promotes Mac-1 receptor activation and inflammation, *Nat. Nanotechnol.*, 2011, **6**(1), 39–44, DOI: **10.1038/nnano.2010.250**.

14 S. Goy-López, J. Juárez, M. Alatorre-Meda, *et al.*, Physicochemical Characteristics of Protein–NP Bioconjugates: The Role of Particle Curvature and Solution Conditions on Human Serum Albumin Conformation and Fibrillogenesis Inhibition, *Langmuir*, 2012, **28**(24), 9113–9126, DOI: **10.1021/la300402w**.

15 S. Tenzer, D. Docter, S. Rosfa, *et al.*, Nanoparticle Size Is a Critical Physicochemical Determinant of the Human Blood Plasma Corona: A Comprehensive Quantitative Proteomic Analysis, *ACS Nano*, 2011, **5**(9), 7155–7167, DOI: 10.1021/nn201950e.

16 M. Li, S. Jiang, J. Simon, *et al.*, Brush Conformation of Polyethylene Glycol Determines the Stealth Effect of Nanocarriers in the Low Protein Adsorption Regime, *Nano Lett.*, 2021, **21**(4), 1591–1598, DOI: 10.1021/acs.nanolett.0c03756.

17 M. Rahmati and M. Mozafari, Protein adsorption on polymers, *Mater. Today Commun.*, 2018, **17**, 527–540, DOI: 10.1016/j.mtcomm.2018.10.024.

18 D. Hühn, K. Kantner, C. Geidel, *et al.*, Polymer-Coated Nanoparticles Interacting with Proteins and Cells: Focusing on the Sign of the Net Charge, *ACS Nano*, 2013, **7**(4), 3253–3263, DOI: 10.1021/nn3059295.

19 M. Ndumiso, N. Buchtová, L. Husselmann, *et al.*, Comparative whole corona fingerprinting and protein adsorption thermodynamics of PLGA and PCL nanoparticles in human serum, *Colloids Surf., B*, 2020, **188**, 110816, DOI: 10.1016/j.colsurfb.2020.110816.

20 C. D. Walkey, J. B. Olsen, F. Song, *et al.*, Protein Corona Fingerprinting Predicts the Cellular Interaction of Gold and Silver Nanoparticles, *ACS Nano*, 2014, **8**(3), 2439–2455, DOI: 10.1021/nn406018q.

21 V. H. Nguyen and B. J. Lee, Protein corona: a new approach for nanomedicine design, *Int. J. Nanomed.*, 2017, **12**, 3137–3151, DOI: 10.2147/IJN.S129300.

22 Y. Zhu, W. Li, Q. Li, *et al.*, Effects of serum proteins on intracellular uptake and cytotoxicity of carbon nanoparticles, *Carbon*, 2009, **47**(5), 1351–1358, DOI: 10.1016/j.carbon.2009.01.026.

23 M. Mahmoudi, N. Bertrand, H. Zope and O. C. Farokhzad, Emerging understanding of the protein corona at the nano-bio interfaces, *Nano Today*, 2016, **11**(6), 817–832, DOI: 10.1016/j.nantod.2016.10.005.

24 A. Salvati, A. S. Pitek and M. P. Monopoli, Transferrin-functionalized nanoparticles lose their targeting capabilities when a biomolecule corona adsorbs on the surface, *Nat. Nanotechnol.*, 2013, **8**, 137–143, DOI: 10.1038/nnano.2012.237.

25 S. Li, C. Cortez-Jugo, Y. Ju and F. Caruso, Approaching Two Decades: Biomolecular Coronas and Bio–Nano Interactions, *ACS Nano*, 2024, **18**(49), 33257–33263, DOI: 10.1021/acsnano.4c13214.

26 Y. Su, X. Fu, L. Wei, Z. Zhang, Q. Zou and F. Cui, PROTCROWN: A Manually Curated Resource of Protein Corona Data for Unlocking the Potential of Protein–Nanoparticle Interactions, *Nano Lett.*, 2025, **25**(5), 1739–1744, DOI: 10.1021/acs.nanolett.4c05955.

27 M. D. Ghouri, A. Tariq, J. Saleem, A. Muhaymin, R. Cai and C. Chen, Protein corona potentiates the recovery of nanoparticle-induced disrupted tight junctions in endothelial cells, *Nanoscale Horiz.*, 2025, **10**(1), 179–189, DOI: 10.1039/d4nh00178h.

28 J. Huzar, R. Coreas, M. P. Landry and G. Tikhomirov, AI-Based Prediction of Protein Corona Composition on DNA Nanostructures, *ACS Nano*, 2025, **19**(4), 4333–4345, DOI: 10.1021/acsnano.4c12259.

29 M. J. Hajirpour, R. Safavi-Sohi and S. Sharifi, An Overview of Nanoparticle Protein Corona Literature, *Small*, 2023, **19**(36), 2301838, DOI: 10.1002/smll.202301838.

30 J. Li, N. Wu, J. Wu, Y. Wan and C. Liu, Effect of protein adsorption on cell uptake and blood clearance of methoxy poly(ethylene glycol)-poly(caprolactone) nanoparticles, *J. Appl. Polym. Sci.*, 2016, **133**(3), 42884–42893, DOI: 10.1002/app.42884.

31 X. B. Xiong, A. Falamarzian, S. M. Garg and A. Lavasanifar, Engineering of amphiphilic block copolymers for polymeric micellar drug and gene delivery, *J. Controlled Release*, 2011, **155**(2), 248–261, DOI: 10.1016/j.jconrel.2011.04.028.

32 M. Chountoulesi, D. Selianitis, S. Pispas and N. Pippa, Recent Advances on PEO-PCL Block and Graft Copolymers as Nanocarriers for Drug Delivery Applications, *Materials*, 2023, **16**(6), 2298, DOI: 10.3390/ma16062298.

33 S. M. Garg, I. M. Paiva, M. R. Vakili, *et al.*, Traceable PEO-poly(ester) micelles for breast cancer targeting: The effect of core structure and targeting peptide on micellar tumor accumulation, *Biomaterials*, 2017, **144**, 17–29, DOI: 10.1016/j.biomaterials.2017.08.001.

34 X. B. Xiong, Z. Binkhathlan, O. Molavi and A. Lavasanifar, Amphiphilic block co-polymers: Preparation and application in nanodrug and gene delivery, *Acta Biomater.*, 2012, **8**(6), 2017–2033, DOI: 10.1016/j.actbio.2012.03.006.

35 N. Ghasemi, M. R. Vakili and A. Lavasanifar, Cross-linking of triblock copolymers of functionalized poly(caprolactone) and poly(ethylene glycol): The effect on the formation of viscoelastic thermogels, *React. Funct. Polym.*, 2022, **171**, 105167, DOI: 10.1016/j.reactfunctpolym.2022.105167.

36 Y. H. Huang, M. R. Vakili, O. Molavi, *et al.*, Decoration of Anti-CD38 on Nanoparticles Carrying a STAT3 Inhibitor Can Improve the Therapeutic Efficacy Against Myeloma, *Cancers*, 2019, **11**(2), 248, DOI: 10.3390/cancers11020248.

37 T. K. Dash and V. B. Konkimalla, Polymeric Modification and Its Implication in Drug Delivery: Poly-ε-caprolactone (PCL) as a Model Polymer, *Mol. Pharmaceutics*, 2012, **9**(9), 2365–2379, DOI: 10.1021/mp3001952.

38 I. M. de Paiva, M. R. Vakili, A. H. Soleimani, *et al.*, Biodistribution and Activity of EGFR Targeted Polymeric Micelles Delivering a New Inhibitor of DNA Repair to Orthotopic Colorectal Cancer Xenografts with Metastasis, *Mol. Pharmaceutics*, 2022, **19**(6), 1825–1838, DOI: 10.1021/acs.molpharmaceut.1c00918.

39 S. M. Garg, M. R. Vakili and A. Lavasanifar, Polymeric micelles based on poly(ethylene oxide) and α-carbon substituted poly(ε-caprolactone): An *in vitro* study on the effect of core forming block on polymeric micellar stability, biocompatibility, and immunogenicity, *Colloids Surf., B*, 2015, **132**, 161–170, DOI: 10.1016/j.colsurfb.2015.05.015.

40 D. Ahmed, P. W. Eide, I. A. Eilertsen, *et al.*, Epigenetic and genetic features of 24 colon cancer cell lines, *Oncogenesis*, 2013, **2**(9), e71, DOI: 10.1038/oncsis.2013.35.

41 K. A. Heck, H. T. Lindholm, B. Niederdorfer, *et al.*, Characterisation of Colorectal Cancer Cell Lines through Proteomic Profiling of Their Extracellular Vesicles, *Proteomes*, 2023, **11**(1), 3, DOI: 10.3390/proteomes11010003.

42 V. Mirshafiee, R. Kim, M. Mahmoudi and M. L. Kraft, The importance of selecting a proper biological milieu for protein corona analysis *in vitro*: Human plasma *versus* human serum, *Int. J. Biochem. Cell Biol.*, 2016, **75**, 188–195, DOI: 10.1016/j.biocel.2015.11.019.

43 M. Mahmoudi, The need for improved methodology in protein corona analysis, *Nat. Commun.*, 2022, **13**(1), 49, DOI: 10.1038/s41467-021-27643-4.

44 S. Tadjiki, S. Sharifi, A. Lavasanifar and M. Mahmoudi, Advancing *In Situ* Analysis of Biomolecular Corona: Opportunities and Challenges in Utilizing Field-Flow Fractionation, *ACS Bio Med Chem Au*, 2024, **4**(2), 77–85, DOI: 10.1021/acsbiomedchemau.4c00001.

45 A. A. Saei, C. M. Beusch, A. Chernobrovkin, *et al.*, ProTargetMiner as a proteome signature library of anticancer molecules for functional discovery, *Nat. Commun.*, 2019, **10**(1), 5715, DOI: 10.1038/s41467-019-13582-8.

46 A. A. Saei, C. M. Beusch, P. Sabatier, *et al.*, System-wide identification and prioritization of enzyme substrates by thermal analysis, *Nat. Commun.*, 2021, **12**(1), 1296, DOI: 10.1038/s41467-021-21540-6.

47 A. A. Ashkarran, H. Gharibi, D. A. Zeki, *et al.*, Multi-omics analysis of magnetically levitated plasma biomolecules, *Biosens. Bioelectron.*, 2023, **220**, 114862, DOI: 10.1016/j.bios.2022.114862.

48 M. Khoubnasabjafari, M. R. A. Mogaddam, E. Rahimpour, J. Soleymani, A. A. Saei and A. Jouyban, Breathomics: Review of Sample Collection and Analysis, Data Modeling and Clinical Applications, *Crit. Rev. Anal. Chem.*, 2022, **52**(7), 1461–1487, DOI: 10.1080/10408347.2021.1889961.

49 F. Ullah, A. Khan, H. M. Akil and M. Siddiq, Effect of Hydrophilic/Hydrophobic Block Ratio and Temperature on the Surface and Associative Properties of Oxyethylene and Oxybutylene Diblock Copolymers in Aqueous Media, *J. Dispersion Sci. Technol.*, 2015, **36**(12), 1777–1785, DOI: 10.1080/01932691.2015.1019625.

50 W. Li, M. Nakayama, J. Akimoto and T. Okano, Effect of block compositions of amphiphilic block copolymers on the physicochemical properties of polymeric micelles, *Polymer*, 2011, **52**(17), 3783–3790, DOI: 10.1016/j.polymer.2011.06.026.

51 W. Zhou, C. Li, Z. Wang, W. Zhang and J. Liu, Factors affecting the stability of drug-loaded polymeric micelles and strategies for improvement, *J. Nanopart. Res.*, 2016, **18**(9), 275, DOI: 10.1007/s11051-016-3583-y.

52 U. Kedar, P. Phutane, S. Shidhaye and V. Kadam, Advances in polymeric micelles for drug delivery and tumor targeting, *Nanomed. Nanotechnol. Biol. Med.*, 2010, **6**(6), 714–729, DOI: 10.1016/j.nano.2010.05.005.

53 J. S. Lee and J. Feijen, Polymersomes for drug delivery: Design, formation and characterization, *J. Controlled Release*, 2012, **161**(2), 473–483, DOI: 10.1016/j.jconrel.2011.10.005.

54 B. C. Paruchuri, V. Gopal, S. Sarupria and J. Larsen, Toward Enzyme-Responsive Polymersome Drug Delivery, *Nanomedicine*, 2021, **16**(30), 2679–2693, DOI: 10.2217/nnm-2021-0194.

55 L. L. Osorno, A. N. Brandley, D. E. Maldonado, A. Yiantsos, R. J. Mosley and M. E. Byrne, Review of Contemporary Self-Assembled Systems for the Controlled Delivery of Therapeutics in Medicine, *Nanomaterials*, 2021, **11**(2), 278, DOI: 10.3390/nano11020278.

56 S. C. Owen, D. P. Y. Chan and M. S. Shoichet, Polymeric micelle stability, *Nano Today*, 2012, **7**(1), 53–65, DOI: 10.1016/j.nantod.2012.01.002.

57 Y. Y. Won, H. T. Davis and F. S. Bates, Giant Wormlike Rubber Micelles, *Science*, 1999, **283**(5404), 960–963, DOI: 10.1126/science.283.5404.960.

58 H. Sun, S. Wang, P. Y. Dugas, F. D'Agosto and M. Lansalot, Peculiar Behavior of Methyl Methacrylate Emulsion Polymerization-Induced Self-Assembly Mediated by RAFT Using Poly(Methacrylic Acid) Macromolecular Chain Transfer Agent, *Macromol. Rapid Commun.*, 2024, **45**(15), 2400141, DOI: 10.1002/marc.202400141.

59 S. Bhattacharjee, DLS and zeta potential – What they are and what they are not?, *J. Controlled Release*, 2016, **235**, 337–351, DOI: 10.1016/j.jconrel.2016.06.017.

60 S. Pabisch, B. Feichtenschlager, G. Kickelbick and H. Peterlik, Effect of interparticle interactions on size determination of zirconia and silica based systems – A comparison of SAXS, DLS, BET, XRD and TEM, *Chem. Phys. Lett.*, 2012, **521**, 91, DOI: 10.1016/j.cplett.2011.11.049.

61 T. Nishimura, S. Fujii, K. Sakurai, Y. Sasaki and K. Akiyoshi, Manipulating the Morphology of Amphiphilic Graft-Copolymer Assemblies by Adjusting the Flexibility of the Main Chain, *Macromolecules*, 2021, **54**(14), 7003–7009, DOI: 10.1021/acs.macromol.1c01030.

62 D. Gabrielaitis, V. Zitkute, L. Saveikyte, *et al.*, Nanotubes from bacteriophage tail sheath proteins: internalisation by cancer cells and macrophages, *Nanoscale Adv.*, 2023, **5**(14), 3705–3716, DOI: 10.1039/D3NA00166K.

63 S. K. Filippov, R. Khusnutdinov, A. Murmiliuk, *et al.*, Dynamic light scattering and transmission electron microscopy in drug delivery: a roadmap for correct characterization of nanoparticles and interpretation of results, *Mater. Horiz.*, 2023, **10**(12), 5354–5370, DOI: 10.1039/D3MH00717K.

64 D. S. Karaman, D. Desai, R. Senthilkumar, *et al.*, Shape engineering *vs.* organic modification of inorganic nanoparticles as a tool for enhancing cellular internalization, *Nanoscale Res. Lett.*, 2012, **7**(1), 358, DOI: 10.1186/1556-276X-7-358.

65 A. Aliyandi, C. Reker-Smit, R. Bron, I. S. Zuhorn and A. Salvati, Correlating Corona Composition and Cell Uptake to Identify Proteins Affecting Nanoparticle Entry into Endothelial Cells, *ACS Biomater. Sci. Eng.*, 2021, **7**(12), 5573–5584, DOI: 10.1021/acsbiomaterials.1c00804.

66 S. Ritz, S. Schottler and N. Kotman, Protein Corona of Nanoparticles: Distinct Proteins Regulate the Cellular Uptake, *Biomacromolecules*, 2015, **16**(4), 1311–1321, DOI: **10.1021/acs.biomac.5b00108**.

67 T. Glavinovic, G. Thanassoulis, J. de Graaf, P. Couture, R. A. Hegele and A. D. Sniderman, Physiological Bases for the Superiority of Apolipoprotein B Over Low-Density Lipoprotein Cholesterol and Non–High-Density Lipoprotein Cholesterol as a Marker of Cardiovascular Risk, *J. Am. Heart Assoc.*, 2022, **11**(20), e025858, DOI: **10.1161/JAHA.122.025858**.

68 A. Mahmud, X. B. Xiong and A. Lavasanifar, Novel Self-Associating Poly(ethylene oxide)-*block*-poly(ε-caprolactone) Block Copolymers with Functional Side Groups on the Polyester Block for Drug Delivery, *Macromolecules*, 2006, **39**(26), 9419–9428, DOI: **10.1021/ma0613786**.

69 S. M. Garg, X. B. Xiong, C. Lu and A. Lavasanifar, Application of Click Chemistry in the Preparation of Poly(ethylene oxide)-block-poly(ε-caprolactone) with Hydrolyzable Cross-Links in the Micellar Core, *Macromolecules*, 2011, **44**(7), 2058–2066, DOI: **10.1021/ma102548m**.

70 A. Mahmud and A. Lavasanifar, The effect of block copolymer structure on the internalization of polymeric micelles by human breast cancer cells, *Colloids Surf., B*, 2005, **45**(2), 82–89, DOI: **10.1016/j.colsurfb.2005.07.008**.

71 M. Yuan, Y. Wang, X. Li, C. Xiong and X. Deng, Polymerization of Lactides and Lactones. 10. Synthesis, Characterization, and Application of Amino-Terminated Poly(ethylene glycol)-co-poly(ε-caprolactone) Block Copolymer, *Macromolecules*, 2000, **33**(5), 1613–1617, DOI: **10.1021/ma991388p**.

72 D. Szklarczyk, J. H. Morris, H. Cook, *et al.*, The STRING database in 2017: quality-controlled protein–protein association networks, made broadly accessible, *Nucleic Acids Res.*, 2017, **45**(D1), D362–D368, DOI: **10.1093/nar/gkw937**.